Supporting Information

Positional Installation of Unsymmetrical Fluorine Functionalities onto Metal-Organic Frameworks for Efficient Carbon Dioxide Separation under Humid Conditions

Seongwoo Kim,[†,ǁ,¶] Tae-Ung Yoon,[‡,ǁ] Kwang Hyun Oh,[‡] Jaesung Kwak,[§] Youn-Sang Bae,[*,‡] and Min Kim[*,†]

[†]Department of Chemistry, Chungbuk National University, 1 Chungdae-ro, Seowon-gu, Cheongju 28644, Republic of Korea

[‡]Department of Chemical and Biomolecular Engineering, Yonsei University, 50 Yonsei-ro, Seodaemun-gu, Seoul 03722, Republic of Korea

[§]Infectious Diseases Therapeutic Research Center, Korea Research Institute of Chemical Technology (KRICT), 141 Gajeong-ro ,Yuseong-gu, Daejeon 34114, Republic of Korea

[ǁ]These authors equally contributed to this work.

[¶]Present address: Materials Architecturing Research Center, Korea Institute of Science and Technology (KIST), Seoul, 02792, Korea

Table of Contents

General Materials and Methods

Unless otherwise stated, all commercially available reagents, reaction solvents, and NMR solvents were used without additional purification. All the chemical reagents and solvents were purchased from Sigma-Aldrich, TCI, Alfa-Aesar, and Acros chemical companies. NMR solvents were purchased from Cambridge Isotope Laboratories and Eurisotop. All solutions were concentrated using a rotary evaporator and vacuum dried at 0.1−1 Torr. Analytical thin layer chromatography (TLC) was performed on pre-coated silica gel 60 F254 plates (Merck, USA).

^{1}H nuclear magnetic resonance (NMR) spectra were recorded on a Bruker AVANCE 500 NMR spectrometer (500 MHz) or a Bruker AVANCE 400 NMR spectrometer (400 MHz). Chemical shifts were quoted in parts per million (ppm) and referenced to the appropriate solvent peak and/or tetramethylsilane (TMS). The following abbreviations were used to describe peak patterns when appropriate: br = broad, s = singlet, d = doublet, and ddd = doublet of doublet of doublet. Coupling constants, *J*, were reported in Hertz (Hz). ^{13}C NMR spectra were recorded on a Bruker AVANCE 500 NMR spectrometer (125 MHz) or a Bruker AVANCE 400 NMR spectrometer (100 MHz) and were fully ^{1}H-decoupled by broad band decoupling.

High-resolution mass spectra (HRMS) were acquired on a high-resolution Q-TOF mass spectrometer (ionization mode: ESI). IR spectra were collected using a Bruker Alpha spectrometer. Powder X-ray diffraction (PXRD) data were collected on a Rigaku Miniflex 600 diffractometer (40 kV, 15 mA) with a scan speed of 1.0 min/step, a step size of 0.02° in 2θ, and a 2θ range 3–50°.

Computational Approaches

All the calculations were performed with Q-Chem 4.4.[S1] Geometry optimization were performed with M06-2X functional[S2] with 6-311++G** basis set. Electrostatic potentials are mapped on the Van der Waals surface. Basis set superposition error correction was used in binding energy calculations as depicted in the previous literature.[S3] ESP maps and computed structures are illustrated using IQmol[S4] and CYLView,[S5] respectively.

Cartesian coordinates of optimized structures

BDC

C	2.87234	-0.12381	-0.00003
C	1.38365	-0.03368	0.00010
C	0.66282	-1.22678	0.00021
H	1.20402	-2.16486	0.00019
C	-0.72372	-1.19557	0.00034
H	-1.29682	-2.11334	0.00043
C	-1.38365	0.03368	0.00038
C	-2.87234	0.12381	0.00058
O	-3.49258	1.15203	-0.00036
O	-3.46820	-1.08270	-0.00053
H	-4.42267	-0.93043	-0.00121
C	-0.66282	1.22678	0.00026
H	-1.20402	2.16486	0.00029
C	0.72372	1.19557	0.00013
H	1.29682	2.11334	0.00005
O	3.46820	1.08270	-0.00030
H	4.42267	0.93043	-0.00049
O	3.49258	-1.15203	-0.00019

BDC-F

C	2.77870	0.21861	0.00008
C	1.28716	0.20320	0.00009
C	0.58000	-0.99995	0.00013
F	1.22073	-2.16472	0.00021
C	-0.80401	-1.03344	0.00008
H	-1.31259	-1.98832	0.00012
C	-1.50453	0.16716	-0.00001

C	-2.99721	0.19370	-0.00007
O	-3.65601	1.19643	-0.00011
O	-3.53813	-1.03663	-0.00000
H	-4.49901	-0.93066	-0.00002
C	-0.82764	1.38563	-0.00004
H	-1.39863	2.30498	-0.00011
C	0.55638	1.39676	0.00001
H	1.09670	2.33361	-0.00001
O	3.26268	1.47857	0.00029
H	4.22659	1.40872	0.00001
O	3.49238	-0.74285	-0.00060

BDC-F_3

C	2.80981	-0.09837	-0.06174
C	1.31974	0.05689	-0.02492
C	0.51142	-1.06929	0.02477
F	1.04640	-2.27828	0.09892
C	-0.87689	-0.97126	0.03880
F	-1.55829	-2.10573	0.11033
C	-1.48564	0.27709	-0.01429
C	-2.96651	0.50328	-0.00862
O	-3.45599	1.59774	-0.04968
O	-3.68175	-0.62252	0.04575
H	-4.61582	-0.37062	0.04329
C	-0.68588	1.41992	-0.07653
H	-1.15267	2.39520	-0.12592
C	0.68466	1.29768	-0.07550
F	1.42917	2.40035	-0.15980
O	3.41651	0.76416	0.76087
H	4.37115	0.63189	0.67240
O	3.38092	-0.90178	-0.73776

BDC-F_4

C	-2.90397	-0.11372	0.06880
C	-1.40670	-0.03835	0.01539
C	-0.66139	-1.20798	-0.07859
F	-1.25957	-2.38373	-0.19677
C	0.72404	-1.16961	-0.09617

F	1.38165	-2.31302	-0.23510
C	1.40670	0.03849	-0.01525
C	2.90397	0.11385	-0.06862
O	3.50637	0.91476	-0.71861
O	3.47125	-0.81705	0.70484
H	4.43103	-0.73592	0.60885
C	0.66139	1.20813	0.07874
F	1.25957	2.38388	0.19692
C	-0.72404	1.16976	0.09631
F	-1.38163	2.31317	0.23526
O	-3.47128	0.81665	-0.70528
H	-4.43107	0.73516	-0.60969
O	-3.50634	-0.91502	0.71835

1,2,5-Trifluorobenzene-CO_2-stacking conformation

C	-0.47655	-1.33003	0.69197
C	-1.47031	-0.39255	0.48374
F	-2.47437	-0.28264	1.35078
C	-1.43925	0.44607	-0.62230
F	-2.41638	1.34057	-0.78382
C	-0.40888	0.35666	-1.53817
C	0.60428	-0.58006	-1.35034
H	1.42735	-0.67392	-2.04589
C	0.54804	-1.40113	-0.23787
F	1.52200	-2.30171	-0.04355
H	-0.50233	-1.97965	1.55652
H	-0.41052	1.02101	-2.39277
C	2.07322	1.37099	0.61658
O	1.11694	1.62304	1.21339
O	3.03568	1.12782	0.02535

1,2,5-Trifluorobenzene-CO_2-side-on conformation

C	1.40963	-1.11405	0.25169
C	2.46532	-0.30765	-0.14194
F	3.64745	-0.88804	-0.39209
C	2.34669	1.06260	-0.28456
H	3.20316	1.64536	-0.59488
C	1.11645	1.65735	-0.02134

C	0.05216	0.87272	0.37371
F	-1.14412	1.41763	0.63161
C	0.19996	-0.49967	0.50754
F	-0.85621	-1.22468	0.88841
H	1.52292	-2.18508	0.35553
H	0.97137	2.72569	-0.12001
C	-2.99898	-0.26957	-0.62674
O	-3.79513	-0.27654	0.20793
O	-2.21348	-0.26602	-1.47570

1,2,4,5-Tetrafluorobenzene-CO_2-stacking conformation

C	0.56215	0.95472	1.20788
C	1.60051	0.33895	0.53374
F	2.74533	0.07913	1.16200
C	1.46180	-0.02079	-0.79848
F	2.47722	-0.61607	-1.42139
C	0.28350	0.22909	-1.47893
C	-0.75549	0.84882	-0.80589
F	-1.89952	1.10847	-1.43459
C	-0.61704	1.20458	0.52841
F	-1.63693	1.79181	1.15395
H	0.66639	1.23007	2.24927
H	0.17821	-0.04969	-2.51943
C	-1.41977	-1.98953	0.45484
O	-0.37978	-2.24363	0.89009
O	-2.45939	-1.73707	0.02003

1,2,4,5-Tetrafluorobenzene-CO_2-side-on conformation

C	-0.98322	-1.40032	-0.21591
C	-2.13076	-0.68833	0.08447
F	-3.25895	-1.33398	0.37679
C	-2.12405	0.69852	0.08622
F	-3.24582	1.35440	0.38039
C	-0.96975	1.40003	-0.21289
C	0.17469	0.68721	-0.51417
F	1.31102	1.32714	-0.80623
C	0.16820	-0.69808	-0.51558
F	1.29838	-1.34796	-0.80772

H	-0.98809	-2.48258	-0.21442
H	-0.96425	2.48229	-0.20944
C	3.27923	0.00076	0.71637
O	4.13204	0.03062	-0.05955
O	2.43352	-0.02999	1.50502

Adsorption measurements

Brunauer-Emmett-Teller (BET) Surface Areas and Pore Volumes

N_2 adsorption and desorption isotherms were recorded at 77 K on a 3Flex analyzer (Micromeritics Instruments, USA). Before each measurement, the sample was degassed under vacuum at 423 K for 4 h. [S6] BET surface areas and total pore volumes were derived from the obtained isotherms. The BET surface areas of the samples, determined from two consistency criteria,[S7-S9] were as follows: $0.0754 < P/P_0 < 0.2722$ for UiO-66-NH_2 and $0.0783 < P/P_0 < 0.2710$ for UiO-66-(NH_2)/(F_3)-CS. The total pore volumes were determined at $P/P_0 = 0.95$.

H_2O adsorption

The H_2O adsorption isotherms were obtained on a 3Flex analyzer (Micromeritics Instruments, USA) at a constant temperature (298 K), maintained using a specially crafted air circulation system (Protech Korea Instruments, Korea). Before each measurement, approximately 100 mg of sample was degassed at 423 K for 4 h.

Breakthrough experiments

The dynamic breakthrough experiments were carried out in a custom-built, fixed-bed system.[S10-S12] Five mass flow controllers (0–100 mL/min) (Bronkhorst, Germany) were used to regulate the gas flow rates. Four of them were used for pure N_2 and CO_2 streams, which were mixed well with each other by flowing through a gas mixer. The first combination produces a dry, CO_2/N_2 mixture and the second combination proceeds through a humidifier to give humid CO_2/N_2 mixtures. The last mass flow controller was used for a He stream for the in-situ regeneration of the adsorbent packed in the column. The column was placed in a ventilated thermostatted oven for measurements at a constant temperature. The composition of the gas flow at the outlet of the column was measured online by a mass spectrometer (Max300-LG Extrel, USA).

To avoid large pressure drops, the as-synthesized powder samples were pelletized into binderless pellets with a size of 500–1000 μm using a carver press (Carver, Inc., USA). The obtained pellets were initially degassed at 423 K for 4 h under vacuum and then packed into a stainless-steel column (15 cm × 0.44 cm). The remainder of the column was filled with glass beads with a diameter of 750 μm.

Before the breakthrough experiments, the column was degassed using a He flow of 40 mL/min at 423 K for 1 h to remove any adsorbed impurities during the packing procedure. The experiment was carried out at 298 K and 1 bar. At $t = 0$, the He flow was switched to the CO_2/N_2 mixture (CO_2:N_2 = 15:85, total flow rate = 20 mL/min).

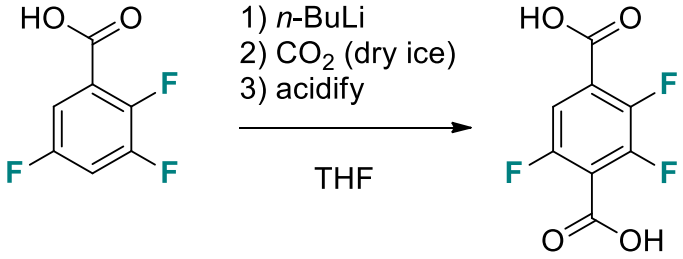

Scheme S1. Synthetic procedure for BDC-F_3.

	Trifluoro ligand	Tetrafluoro ligand
Stacking conformation	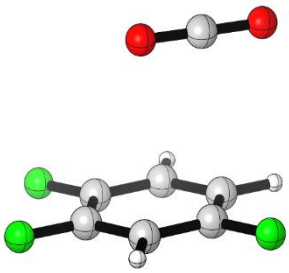 BE: -9.0 kJ/mol	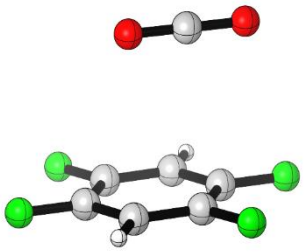 BE: -7.0 kJ/mol
Side-on conformation	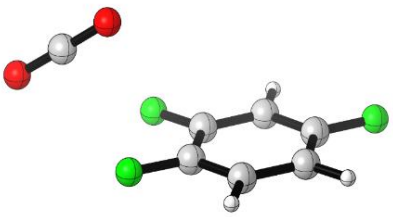 BE: -10.9 kJ/mol	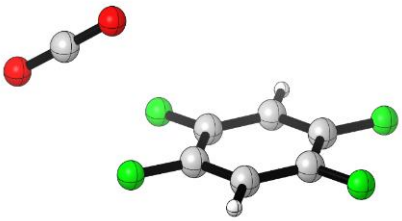 BE: -10.6 kJ/mol

Figure S1. Binding energy (BE) differences of trifluoro and tetrafluoro ligands with carbon dioxide.

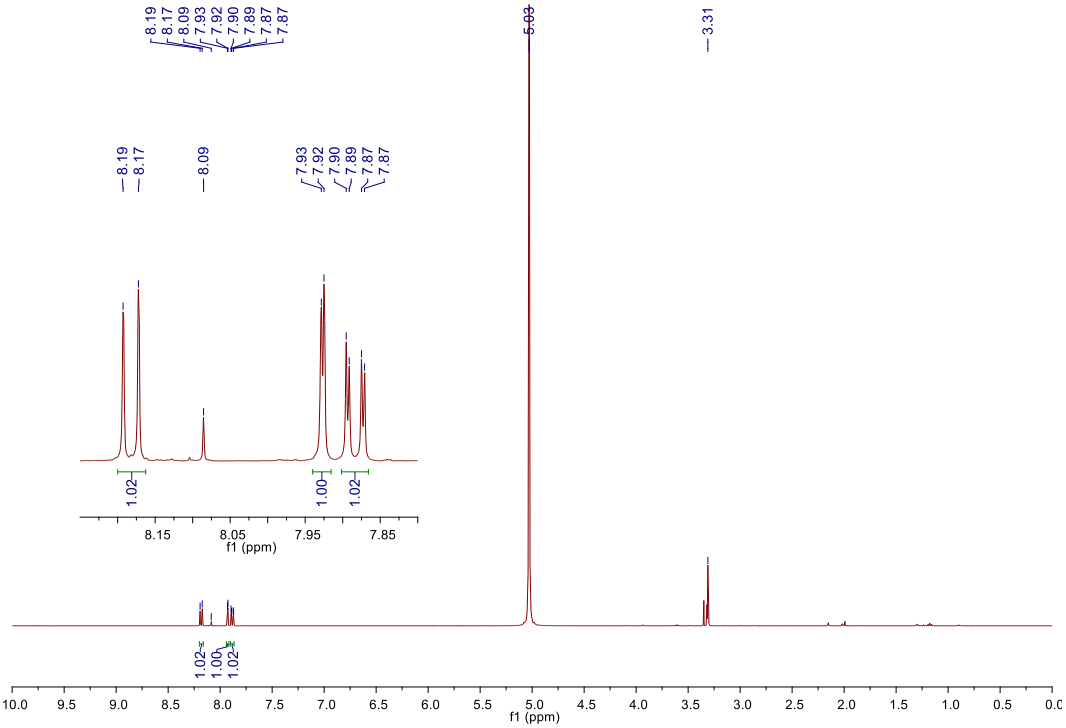

Figure S2. ^{1}H NMR spectrum of UiO-66-NH_2 after acid digestion.

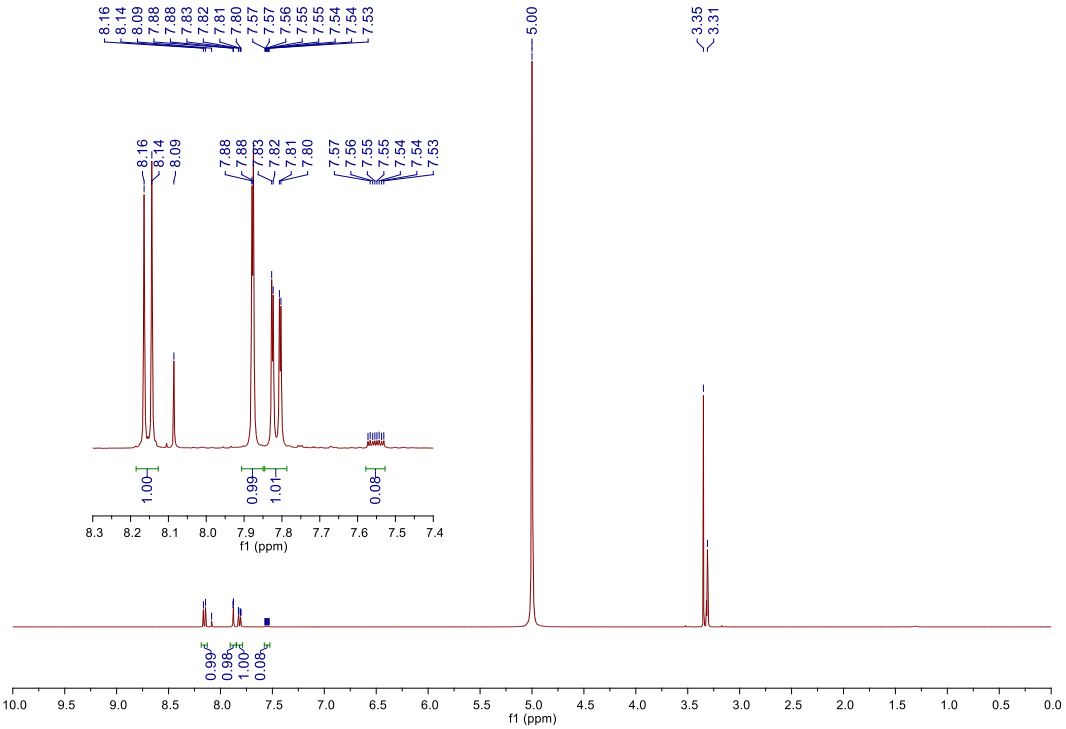

Figure S3. ^{1}H NMR spectrum of mixed UiO-66-(NH_2)(F_3) after acid digestion.

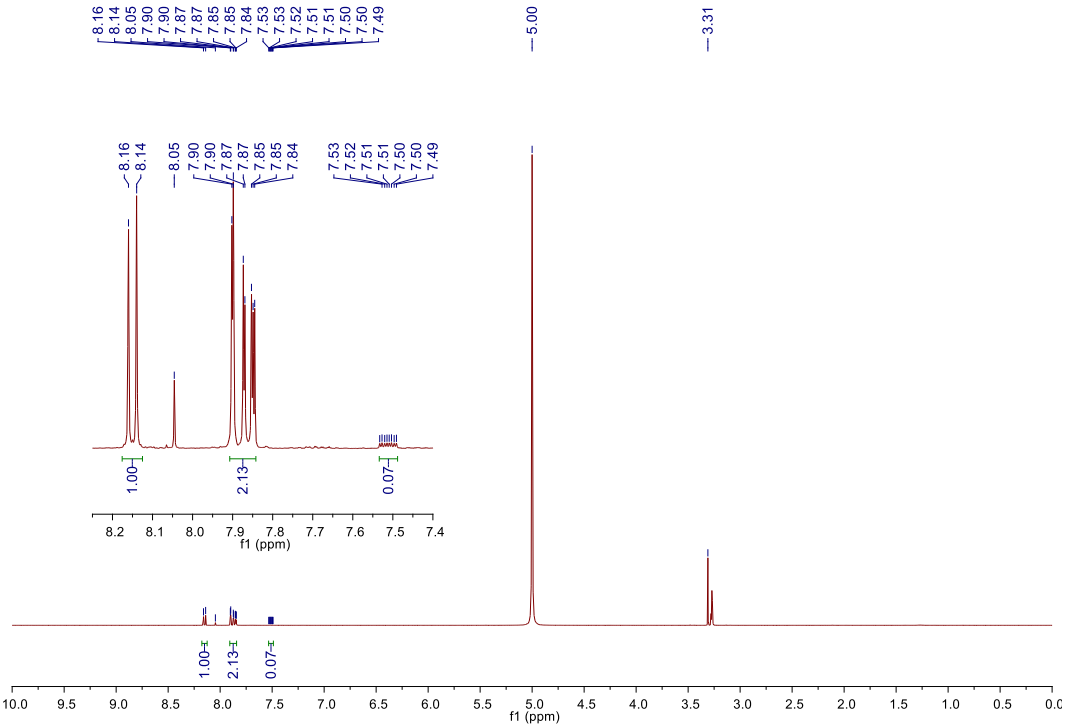

Figure S4. ^{1}H NMR spectrum of UiO-66-(NH_2)/(F_3)-CS after acid digestion.

	UiO-66-(NH_2)(F_3)	UiO-66-(NH_2)/(F_3)-CS
SEM	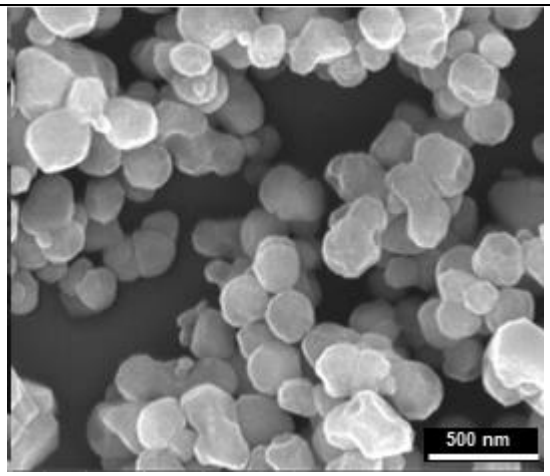	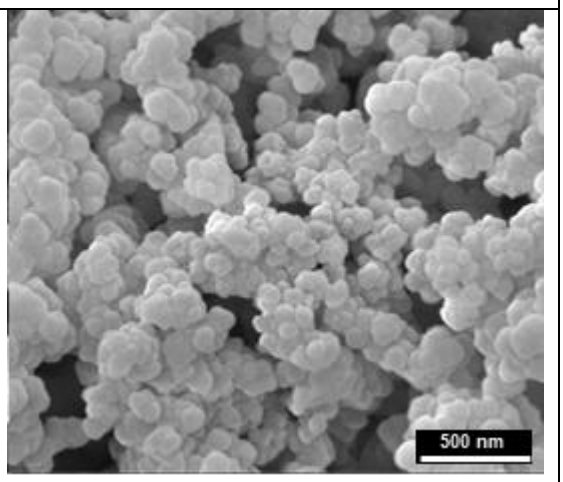
SEM-EDX	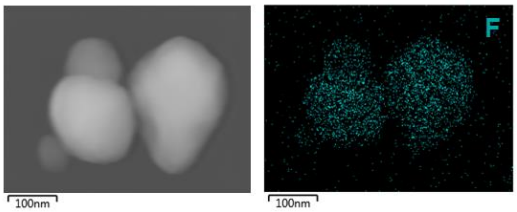	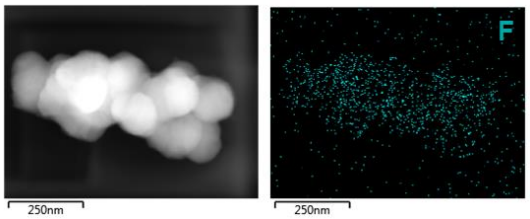
TEM-EDX	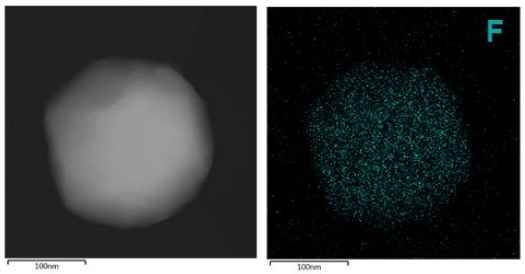	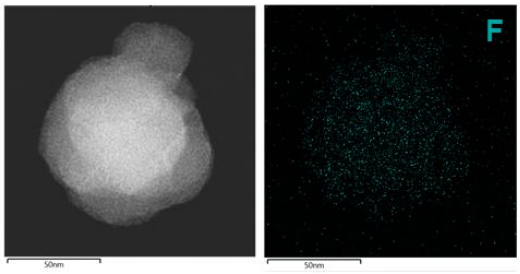

Figure S5. SEM, SEM-EDX, and TEM-EDX of UiO-66-(NH_2)(F_3) and UiO-66-(NH_2)/(F_3)-CS.

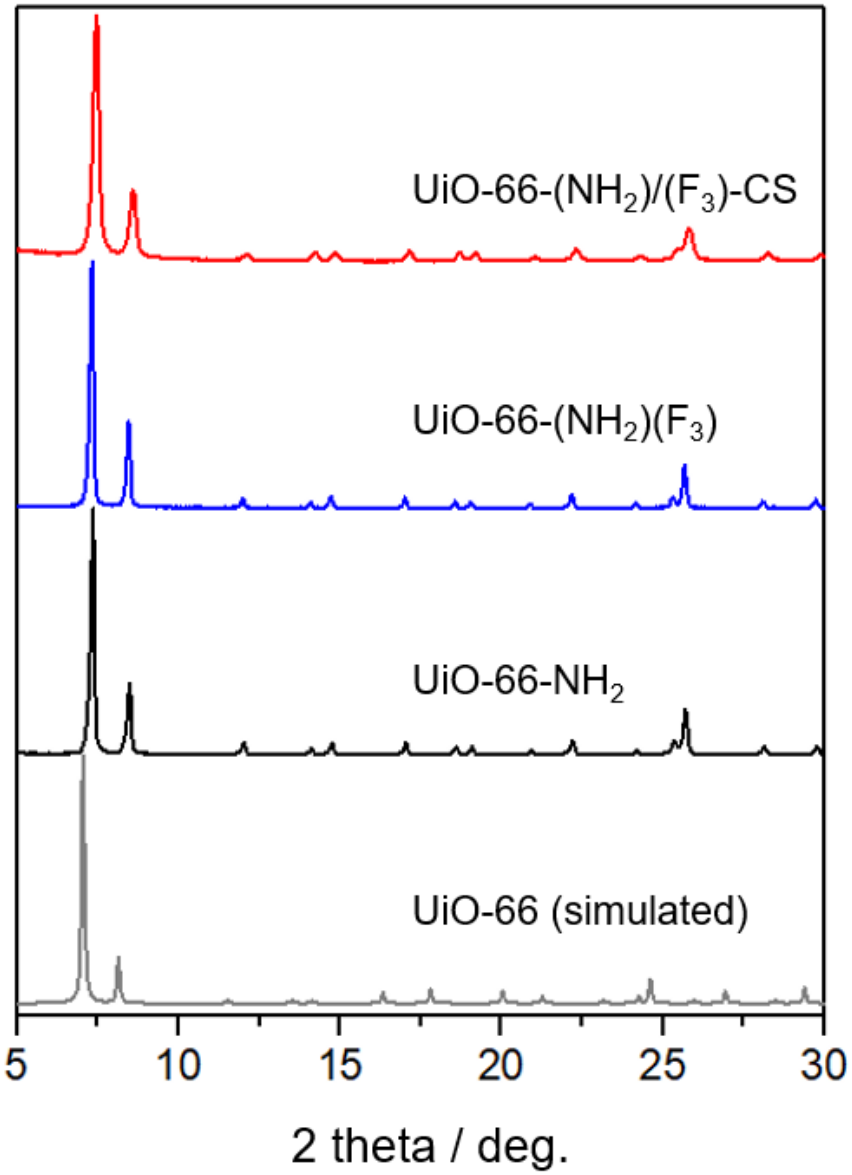

Figure S6. Powder X-ray diffraction (PXRD) patterns of UiO-66-NH_2, UiO-66-(NH_2)(F_3) and UiO-66-(NH_2)/(F_3)-CS.

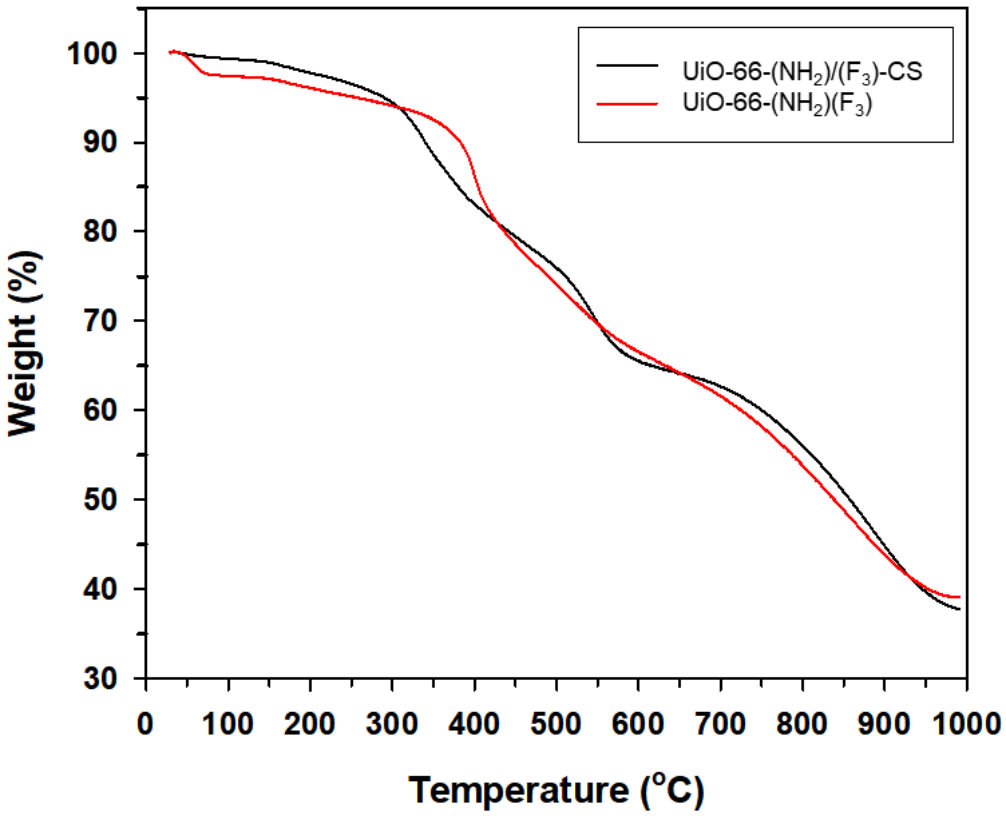

Figure S7. Thermogravimetry analysis of UiO-66-(NH_2)(F_3) and UiO-66-(NH_2)/(F_3)-CS.

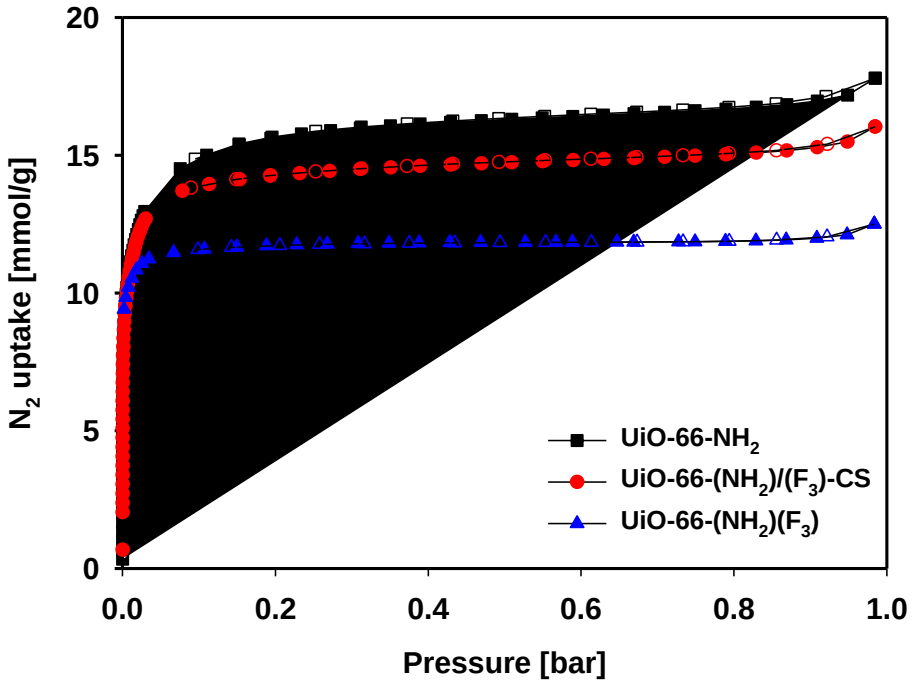

Figure S8. N_2 adsorption-desorption equilibrium isotherms at 77 K of UiO-66-NH_2, UiO-66-$(NH_2)/(F_3)$-CS and UiO-66-$(NH_2)(F_3)$.

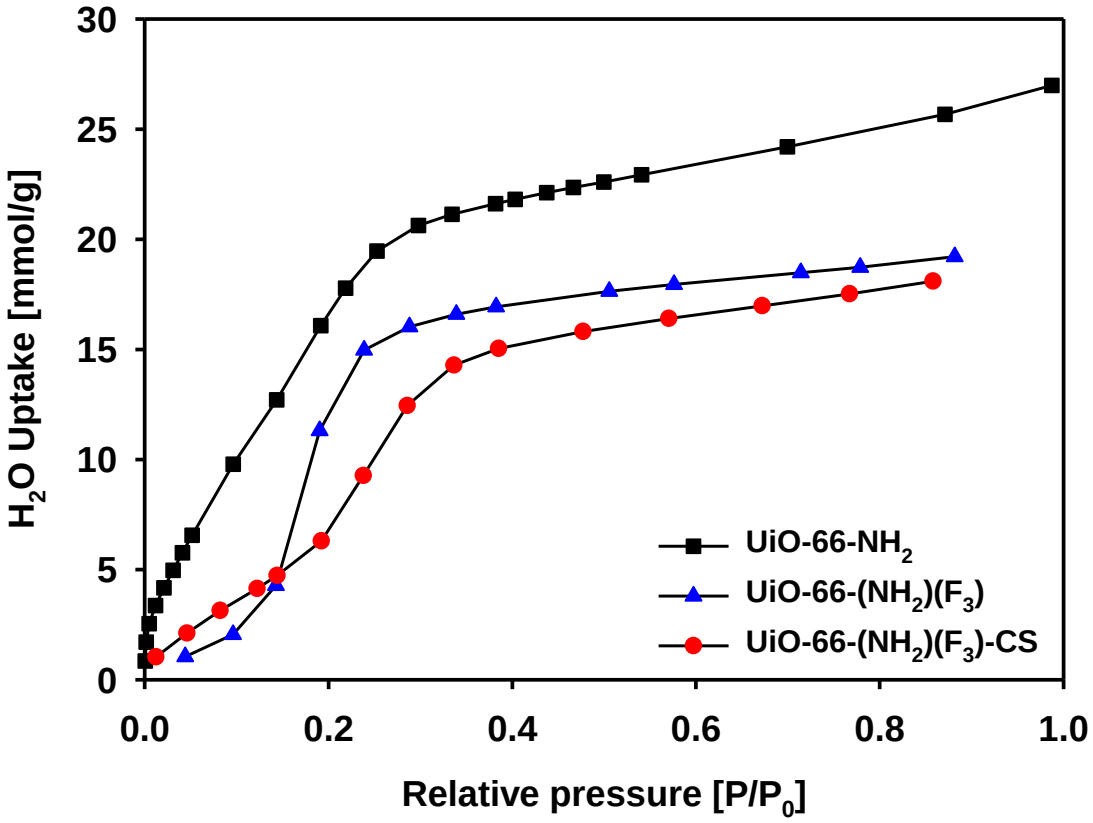

Figure S9. H_2O adsorption isotherms of UiO-66-NH_2, UiO-66-(NH_2)/(F_3)-CS and UiO-66-(NH_2)(F_3) at 298 K.

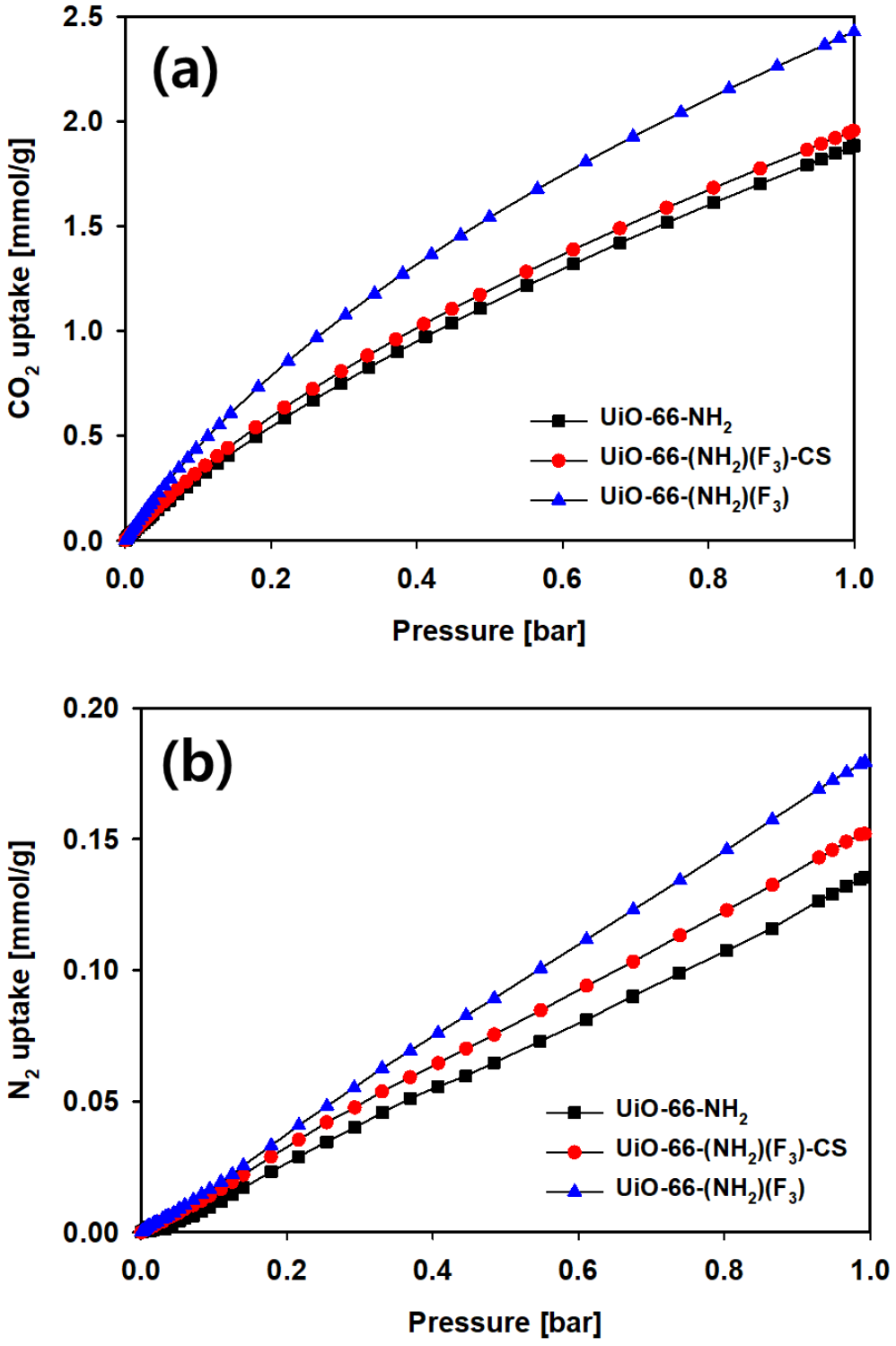

Figure S10. CO_2 (a) and N_2 (b) adsorption isotherms at 298 K for UiO-66-NH_2, UiO-66-(NH_2)/(F_3)-CS and UiO-66-$(NH_2)(F_3)$.

Table S1. Textural properties of UiO-66-NH_2, UiO-66-(NH_2)/(F_3)-CS and UiO-66-(NH_2)(F_3).

	BET surface area (m^2/g)	Total pore volume (cm^3/g)
UiO-66-NH_2	1,336	0.60
UiO-66-(NH_2)/(F_3)-CS	1,221	0.54
UiO-66-(NH_2)(F_3)	1,047	0.45

Table S2. Henry adsorption constants (H; mmol g^{-1} bar^{-1}) for CO_2 in UiO-66-NH_2, UiO-66-(NH_2)/(F_3) and UiO-66-(NH_2)/(F_3)-CS at 298 K.

MOF	H (CO_2)
UiO-66-NH_2	3.98
UiO-66-(NH_2)(F_3)	5.57
UiO-66-(NH_2)/(F_3)-CS	4.04

References for Supporting Information

(S1) Shao, Y.; Gan, Z.; Epifanovsky, E.; Gilbert, A. T. B.; Wormit, M.; Kussmann, J.; Lange, A. W.; Behn, A.; Deng, J.; Feng, X.; Ghosh, D.; Goldey, M.; Horn, P. R.; Jacobson, L. D.; Kaliman, I.; Khaliullin, R. Z.; Kuš, T.; Landau, A.; Liu, J.; Proynov, E. I.; Rhee, Y. M.; Richard, R. M.; Rohrdanz, M. A.; Steele, R. P.; Sundstrom, E. J.; Woodcock, H. L.; Zimmerman, P. M.; Zuev, D.; Albrecht, B.; Alguire, E.; Austin, B.; Beran, G. J. O.; Bernard, Y. A.; Berquist, E.; Brandhorst, K.; Bravaya, K. B.; Brown, S. T.; Casanova, D.; Chang, C. M.; Chen, Y.; Chien, S. H.; Closser, K. D.; Crittenden, D. L.; Diedenhofen, M.; Distasio, R. A.; Do, H.; Dutoi, A. D.; Edgar, R. G.; Fatehi, S.; Fusti-Molnar, L.; Ghysels, A.; Golubeva-Zadorozhnaya, A.; Gomes, J.; Hanson-Heine, M. W. D.; Harbach, P. H. P.; Hauser, A. W.; Hohenstein, E. G.; Holden, Z. C.; Jagau, T. C.; Ji, H.; Kaduk, B.; Khistyaev, K.; Kim, J.; Kim, J.; King, R. A.; Klunzinger, P.; Kosenkov, D.; Kowalczyk, T.; Krauter, C. M.; Lao, K. U.; Laurent, A. D.; Lawler, K. V.; Levchenko, S. V.; Lin, C. Y.; Liu, F.; Livshits, E.; Lochan, R. C.; Luenser, A.; Manohar, P.; Manzer, S. F.; Mao, S. P.; Mardirossian, N.; Marenich, A. V.; Maurer, S. A.; Mayhall, N. J.; Neuscamman, E.; Oana, C. M.; Olivares-Amaya, R.; Oneill, D. P.; Parkhill, J. A.; Perrine, T. M.; Peverati, R.; Prociuk, A.; Rehn, D. R.; Rosta, E.; Russ, N. J.; Sharada, S. M.; Sharma, S.; Small, D. W.; Sodt, A.; Stein, T.; Stück, D.; Su, Y. C.; Thom, A. J. W.; Tsuchimochi, T.; Vanovschi, V.; Vogt, L.; Vydrov, O.; Wang, T.; Watson, M. A.; Wenzel, J.; White, A.; Williams, C. F.; Yang, J.; Yeganeh, S.; Yost, S. R.; You, Z. Q.; Zhang, I. Y.; Zhang, X.; Zhao, Y.; Brooks, B. R.; Chan, G. K. L.; Chipman, D. M.; Cramer, C. J.; Goddard, W. A.; Gordon, M. S.; Hehre, W. J.; Klamt, A.; Schaefer, H. F.; Schmidt, M. W.; Sherrill, C. D.; Truhlar, D. G.; Warshel, A.; Xu, X.; Aspuru-Guzik, A.; Baer, R.; Bell, A. T.; Besley, N. A.; Chai, J. Da; Dreuw, A.; Dunietz, B. D.; Furlani, T. R.; Gwaltney, S. R.; Hsu, C. P.; Jung, Y.; Kong, J.; Lambrecht, D. S.; Liang, W.; Ochsenfeld, C.; Rassolov, V. A.; Slipchenko, L. V.; Subotnik, J. E.; Van Voorhis, T.; Herbert, J. M.; Krylov, A. I.; Gill, P. M. W.; Head-Gordon, M. Advances in Molecular Quantum Chemistry Contained in the Q-Chem 4 Program Package. *Mol. Phys.* **2015**, *113*, 184–215.

(S2) Chen, L.; Cao, F.; Sun, H. Ab Initio Study of the π-π Interactions between CO2 and Benzene, Pyridine, and Pyrrole. *Int. J. Quantum Chem.* **2013**, *113*, 2261–2266.

(S3) Zhao, Y.; Truhlar, D. G. Comparative DFT Study of van Der Waals Complexes: Rare-Gas Dimers, Alkaline-Earth Dimers, Zinc Dimer and Zinc-Rare-Gas Dimers. *J. Phys. Chem. A* **2006**, *110*, 5121–5129.

(S4) Legault, C. T. CYL View, version 1.0 b; Universite de Sherbrooke, Sherbrooke, Quebec, Canada, 2009; http://www.cylview.org.

(S5) Rouquerol, J.; Llewellyn, P.; Rouquerol, F. *Stud. Surf. Sci. Catal.* **2007**, *160*, 49-56.

(S6) Katz, M. J.; Brown, Z. J.; Colon, Y. J.; Siu, P. W.; Scheidt, K. A.; Snurr, R. Q.; Hupp, J. T.; Farha, O. K. A facile synthesis of UiO-66, UiO-67 and their derivatives. *Chem. Commun.* **2013**. *49*. 9449-9451.

(S7) Walton, K. S.; Snurr, R. Q. Applicability of the BET Method for Determining Surface Areas of Microporous Metal-Organic Frameworks. *J. Am. Chem. Soc.* **2007**, *129*, 8552–8556.

(S8) Bae, Y. S.; Yazayd'n, A. Ö.; Snurr, R. Q. Evaluation of the BET Method for Determining Surface Areas of MOFs and Zeolites That Contain Ultra-Micropores. *Langmuir* **2010**, *26*, 5475–5483.

(S9) Lee, S. J.; Yoon, T. U.; Kim, A. R.; Kim, S. Y.; Cho, K. H.; Hwang, Y. K.; Yeon, J. W.; Bae, Y. S. Adsorptive Separation of Xenon/Krypton Mixtures Using a Zirconium-Based Metal-Organic Framework with High Hydrothermal and Radioactive Stabilities. *J. Hazard. Mater.* **2016**, *320*, 513–520.

(S10) Lee, S. J.; Kim, K. C.; Yoon, T. U.; Kim, M. B.; Bae, Y. S. Selective Dynamic Separation of Xe and Kr in Co-MOF-74 through Strong Binding Strength between Xe Atom and Unsaturated Co^{2+} Site. *Microporous Mesoporous Mater.* **2016**, *236*, 284–291.

(S11) Yoon, J. W.; Yoon, T. U.; Kim, E. J.; Kim, A. R.; Jung, T. S.; Han, S. S.; Bae, Y. S. Highly Selective Adsorption of CO over CO_2 in a Cu(I)-Chelated Porous Organic Polymer. *J. Hazard. Mater.* **2018**, *341*, 321–327.

(S12) Lee, S. J.; Kim, S.; Kim, E. J.; Kim, M.; Bae, Y. S. Adsorptive Separation of Xenon/Krypton Mixtures Using Ligand Controls in a Zirconium-Based Metal-Organic Framework. *Chem. Eng. J.* **2018**, *335*, 345–351.

Appendix

^{1}H NMR, ^{13}C NMR, and IR Spectra of the Obtained Compounds

2,3,5-Trifluoroterephthalic acid (BDC-F_3)

(500 MHz ^{1}H NMR in CD_3OD-d_4, 125 MHz ^{13}C NMR in DMSO-d_6)

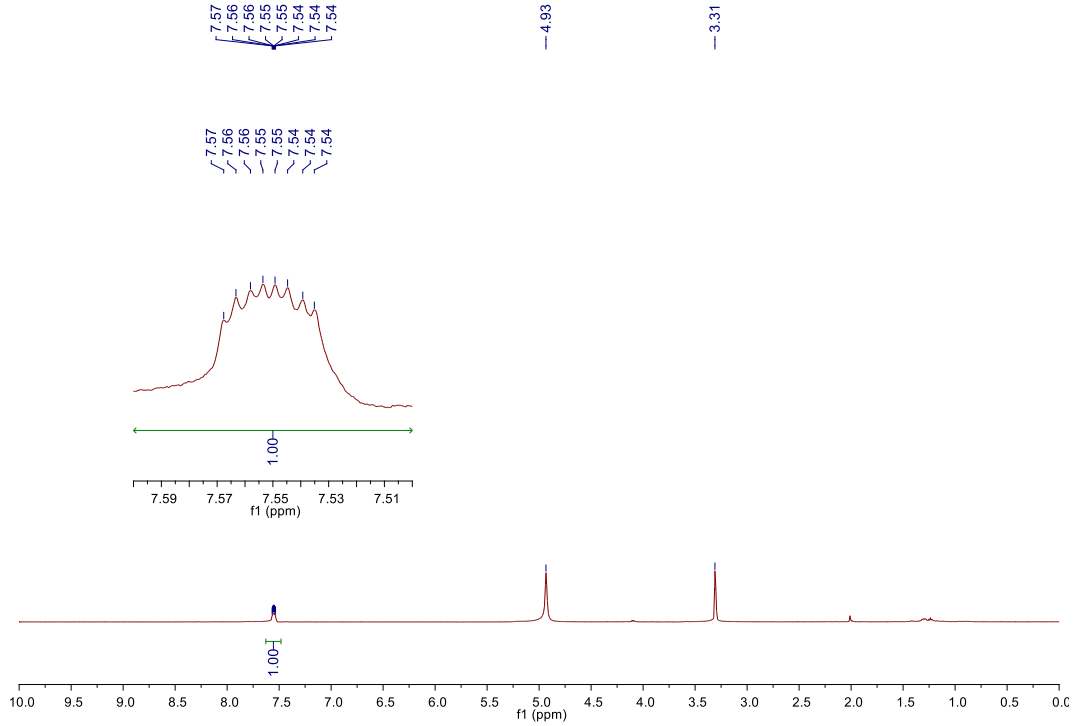

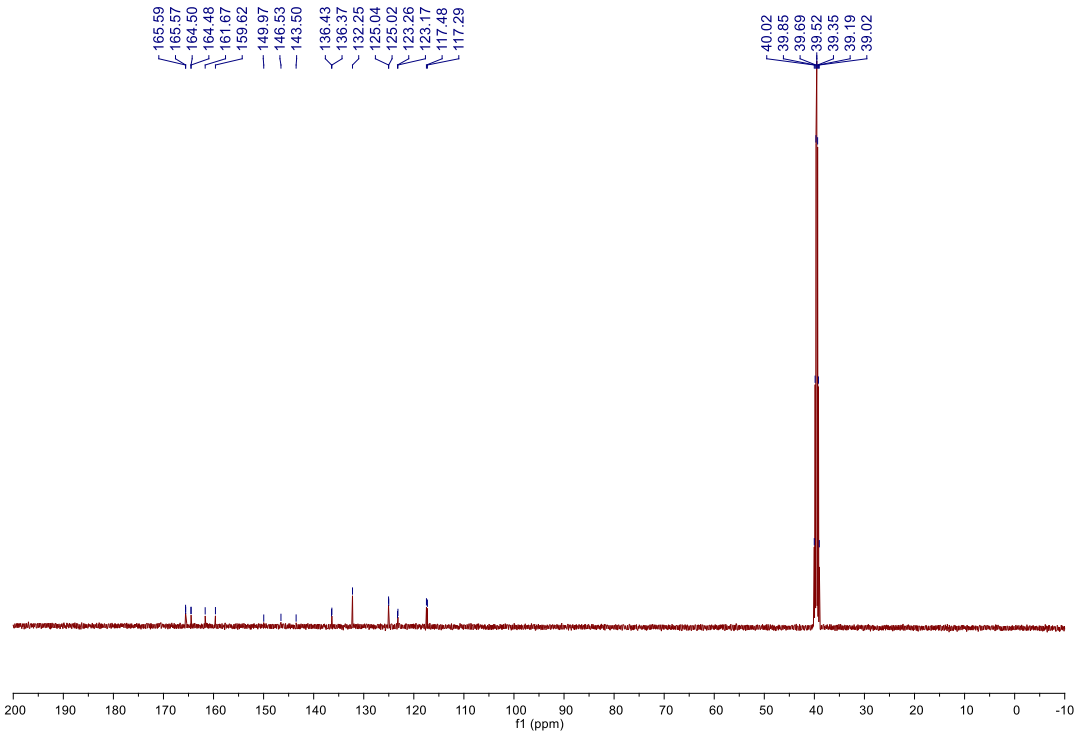

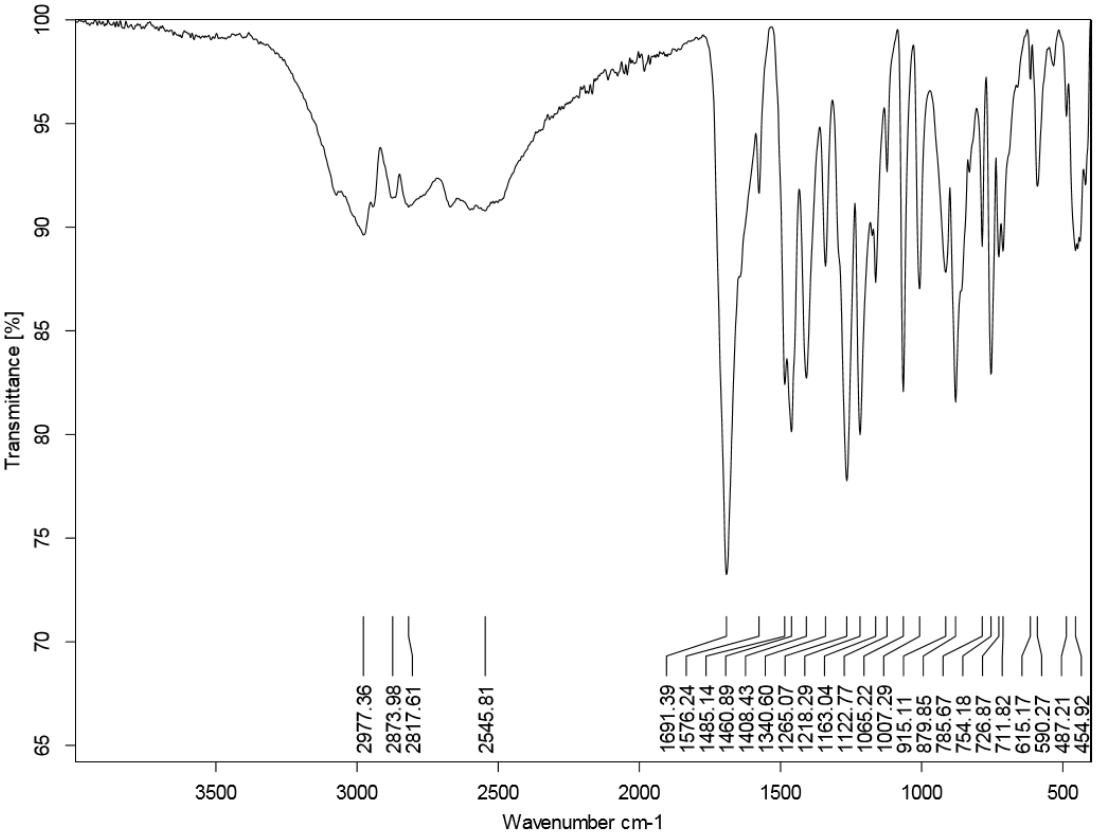
Transmittance [%]
100
95
90
85
80
75
70
65
3500
3000
2500
2000
1500
1000
500
Wavenumber cm-1
2977.36
2873.98
2817.61
2545.81
1691.39
1576.24
1485.14
1460.89
1408.43
1340.60
1265.07
1218.29
1163.04
1122.77
1065.22
1007.29
915.11
879.85
785.67
754.18
726.87
711.82
615.17
590.27
487.21
454.92